AGU PUBLICATIONS

Geophysical Research Letters

RESEARCH LETTER
10.1002/2017GL076548

Key Points:
- The low-frequency variance of the main Pacific climate modes might increase under anthropogenic forcing
- The coupling between ENSO and the Pacific Meridional mode increases under anthropogenic forcing

Supporting Information:
- Supporting Information S1

Correspondence to:
G. Liguori,
giovanni.liguori@gatech.edu

Citation:
Liguori, G., & Di Lorenzo, E. (2018). Meridional modes and increasing Pacific decadal variability under anthropogenic forcing. *Geophysical Research Letters*, *45*. https://doi.org/10.1002/2017GL076548

Received 22 AUG 2017
Accepted 28 DEC 2017
Accepted article online 8 JAN 2018

Meridional Modes and Increasing Pacific Decadal Variability Under Anthropogenic Forcing

Giovanni Liguori[1] **and Emanuele Di Lorenzo**[1]

[1]School of Earth and Atmospheric Sciences, Georgia Institute of Technology, Atlanta, GA, USA

Abstract Pacific decadal variability has strong impacts on the statistics of weather, atmosphere extremes, droughts, hurricanes, marine heatwaves, and marine ecosystems. Sea surface temperature (SST) observations show that the variance of the El Niño-like decadal variability has increased by ~30% (1920–2015) with a stronger coupling between the major Pacific climate modes. Although we cannot attribute these trends to global climate change, the examination of 30 members of the Community Earth System Model Large Ensemble (LENS) forced with the RCP8.5 radiative forcing scenario (1920–2100) suggests that significant anthropogenic trends in Pacific decadal variance will emerge by 2020 in response to a more energetic North Pacific Meridional Mode (PMM)—a well-known El Niño precursor. The PMM is a key mechanism for energizing and coupling tropical and extratropical decadal variability. In the LENS, the increase in PMM variance is consistent with an intensification of the winds-evaporation-SST thermodynamic feedback that results from a warmer mean climate.

Plain Language Summary Decadal variability modulates weather, droughts, hurricanes, and marine heatwaves in the Pacific Ocean with dramatic societal and ecological impacts. Understanding how decadal variability may change in a warming climate remains difficult to assess because of the limited observational record and poor reproducibility of decadal dynamics in climate projection models. We combine theory with available reanalysis products and a large climate model ensemble, to show that the Pacific decadal variance increases under anthropogenic forcing as a result of stronger thermodynamic coupling between ocean and atmosphere. Given that thermodynamic coupling is also increasing in other ocean basins, this study provides a mechanistic framework to understand the amplification of climate variability on global scales under anthropogenic forcing.

1. Introduction

Understanding how decadal variability of the Pacific may change in the future is of great interest because of its direct and indirect impacts on ecosystems and weather, including ocean and atmosphere extremes (Chavez et al., 2003; Di Lorenzo & Mantua, 2016; Gershunov & Barnett, 1998; Mantua et al., 1997; Roemmich & Mcgowan, 1995). Previous studies examine changes in the Pacific decadal variability (PDV) of sea surface temperatures (SSTs) in the context of Empirical Orthogonal Function (EOF), such as the Pacific Decadal Oscillation (PDO; Mantua et al., 1997). While approaches such as these are useful for characterizing the decadal state of the Pacific basin, they do not provide a mechanistic basis for exploring the sensitivity of PDV to anthropogenic forcing.

Here we use a diagnostic framework of PDV that explains the dominant mode of low-frequency (>8 years) SST variability over the Pacific basin (i.e., the El Niño–Southern Oscillation (ENSO)-like pattern (Zhang, Wallace, & Battisti, 1997)) to explore the past and future changes in PDV across observational products and the Community Earth System Model (CESM) Large Ensemble (LENS). This framework, proposed by Di Lorenzo et al. (2015), decomposes the ENSO-like pattern into a growing, peak, and decaying phase. The growth phase pattern is associated with ENSO precursor dynamics, such as North Pacific Meridional Modes (PMM) (Alexander et al., 2010; Anderson, 2003; Chiang & Vimont, 2004; Zhang et al., 2014) (Figure 1c) and the Trade Wind-induced Charging of the equatorial thermocline (Anderson et al., 2013). The peak phase is associated with the development of ENSO and its teleconnections to the midlatitude (Figure 1d) with a hemispherically symmetric SST footprint, which then decays in both tropics and extratropics (Figure 1e). This progression of events has an inherent timescale between 18 and 24 months and has been proposed as an important mechanism to explain the ENSO-like pattern of low-frequency variance (>8 years) (Di Lorenzo et al., 2015). The advantage of this PDV diagnostic framework lies in the possibility of assessing the extent to which

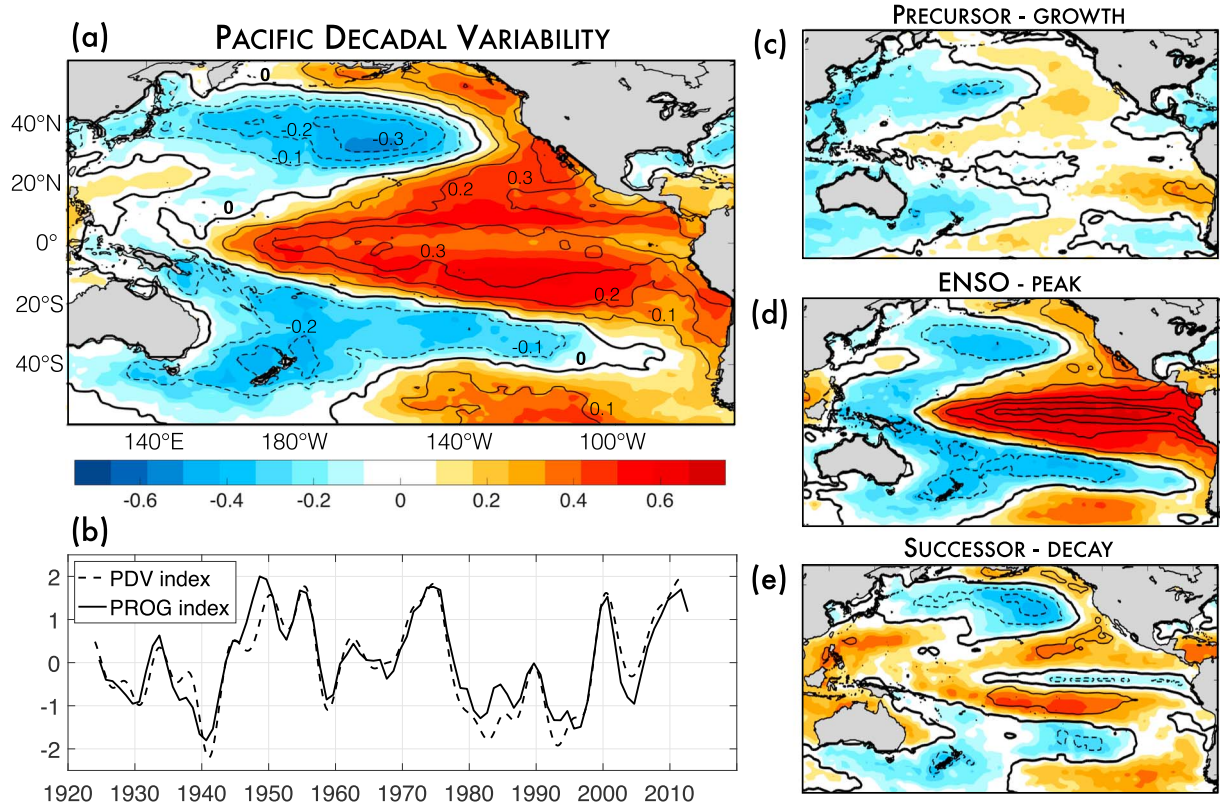

Figure 1. Pacific decadal variability. (a) Correlation and regression maps of the PDV index (i.e., leading PC of 8 year low-passed SST over the Pacific domain) onto 8 year low-passed Pacific SST. Color shading represents the correlation coefficient while the contours represent the regression coefficient. Contour interval 0.1°C per standard deviation of the PDV index. Negative contours are dashed; the zero contour is thickened. (b) The PDV index shown together with the 8 year low-passed PROG index (see text for the definition of the PROG index). As in Figure 1a but at different lags and using unfiltered SSTs and ENSO index (defined as the PC1 of SST anomalies between 20°S and 20°N). When SSTs precede ENSO of 1 year, (c) the precursor, when there is no lag between ENSO and SSTs, (d) the peak, and when ENSO leads the SSTs of 1 year, (e) the successor.

the PDV variance in LENS is consistent with the mechanisms inferred from observations, namely, the interaction between PMM and ENSO.

The main objective of this paper is to use the dynamical framework proposed by Di Lorenzo et al. (2015) to examine the sensitivity of the PDV to anthropogenic forcing. Using observations, we develop a new index that is designed to capture the ENSO-like decadal variability and the progression patterns associated with the growing (PMM), peak (ENSO), and decaying phases of Pacific SST variability. We then use this index to explore projected changes in the PDV variance under the RCP8.5 radiative forcing scenario and assess the role of the PMM.

2. Observations and Modeling

We use two sources of SST data sets, the National Oceanic and Atmospheric Administration Extended Reconstruction SST, version 3 (ERSST v3) product (Smith & Reynolds, 2005) and the Met Office Hadley Centre SST, version 1.1 (HadISST v1.1) data set (Rayner et al., 2003). ERSST v3 (HadISST v1.1) consists of monthly mean values from 1854 (1870) to the present on a 2° × 2° (1° × 1°) horizontal grid globally. Except for SST-only analyses, which use data from 1920 to 2015 (i.e., Figures 1 and 2b), we restrict the period of record to 1950–2015 to match the other data sets. Monthly mean values of sea level pressure (SLP), 10 m wind components (U and V), and latent heat flux (LHF) are taken from the National Centers for Environmental Prediction-National Center for Atmospheric Research reanalysis product (Kalnay et al., 1996) and exist on a 2.5° × 2.5° horizontal grid globally.

To investigate the PDV response under increasing greenhouse forcing, we analyze the output of the first 30 members of the CESM Large Ensemble simulations (hereafter LENS) from 1920 to 2100 under the RCP8.5

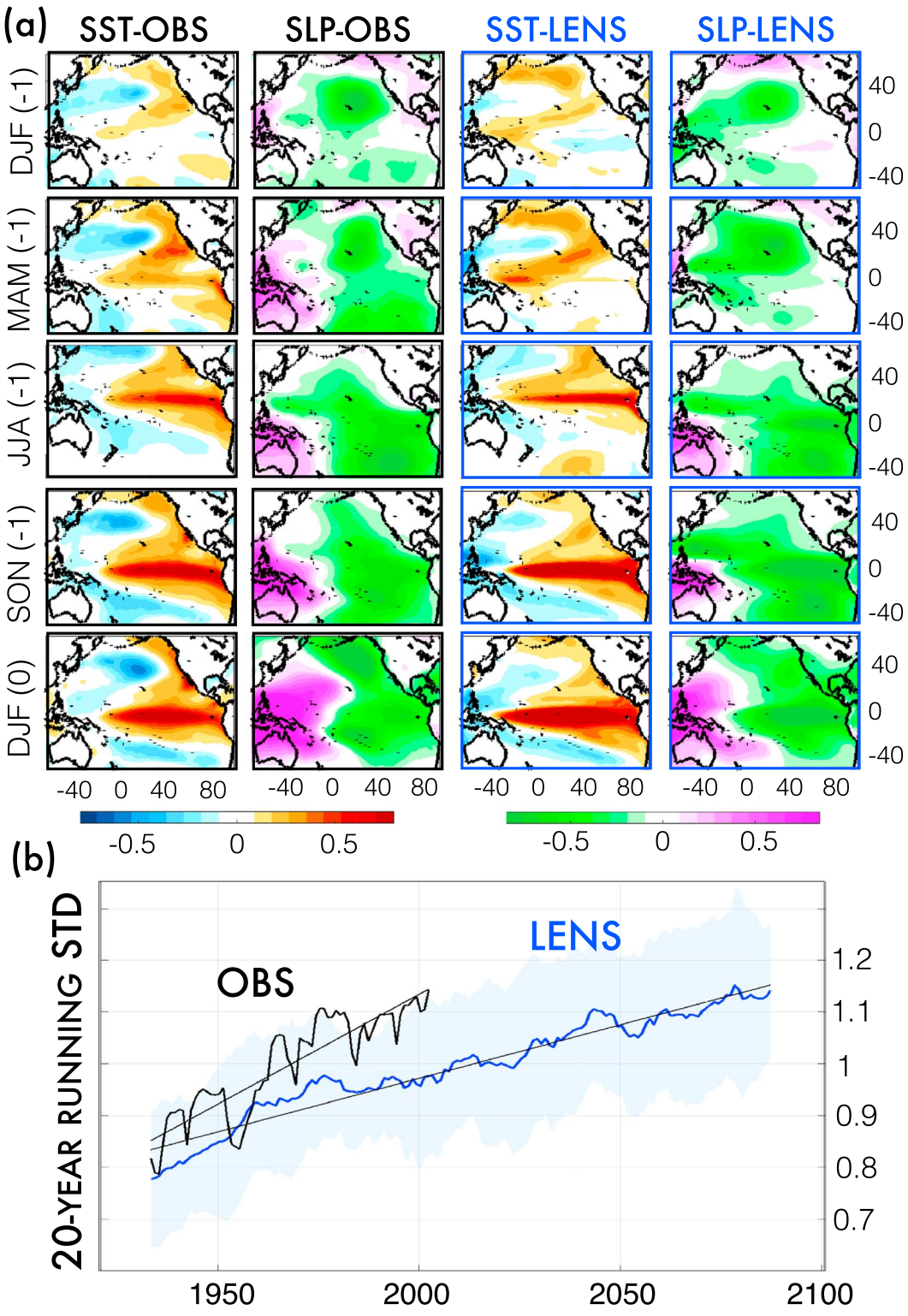

Figure 2. PMM progression (a) seasonal means of SSTa and standardized SLPa regressed onto PROG index in LENS (ensemble mean) and observations**.** Units for SST maps are in °C per units of STD change of PROG index. SLP maps are in units of correlation. (b) Progression strength computed applying a 20 year running STD to the PROG index. Observation (black) and LENS ensemble mean (blue) with its 1 STD spread envelope (shading).

emission scenario available at http://www.cesm.ucar.edu/projects/community-projects/LENS/ (Kay et al., 2015). The 30-member ensemble uses historical radiative forcing for the period 1920–2005 and RCP8.5 radiative forcing thereafter. The simulation uses version 1 of CESM, with the Community Atmosphere Model, version 5 (CESM1(CAM5); Hurrell et al., 2013) at approximately 1° × 1° horizontal resolution in all model components. Unless otherwise stated, monthly mean anomalies are computed by removing the climatological seasonal cycle (computed as long-term monthly mean of the record analyzed) from detrended fields. For the observational data sets, detrended fields are obtained by removing the linear fit at each grid point. For the LENS, they are obtained by removing at each grid point the signal associated with anthropogenic forcing, which is assumed to be the ensemble mean. Although each LENS realization starts with almost identical initial conditions in the ocean subsurface, it is reasonable to assume that each realization develops an independent natural (unforced) multidecadal variability in the Pacific Ocean. In the Pacific, the surface decadal variability is not strongly coupled to the subsurface ocean state (Meehl & Teng, 2012). This contrasts with the Atlantic where the surface decadal variability is linked to the Atlantic Meridional Overturning Circulation (e.g., Delworth & Mann, 2000, and references therein). Thus, averaging all the ensemble members should be effective in extracting the anthropogenic forced signal in the Pacific Ocean. Following Chang et al. (2007), the PMM pattern is obtained as leading maximum covariance analysis (MCA) of boreal spring (defined as March-April-May or MAM) SST and surface wind stress anomaly with the ENSO signal removed by linear regression prior to the analysis. Time series of the PMM are then obtained by projecting the monthly mean anomalies onto the leading MCA spatial pattern. As a result of the projection, we obtain two monthly mean indices, an SST-based index, PMM_{sst}, and a 10 m winds-based index, $PMM_{?}$. The ENSO index is computed as the leading principal component (PC1) of monthly mean tropical Pacific ([120E-80°W, 20S–20°N]) SSTs. All the seasons in this manuscript are boreal seasons.

3. Increasing Pacific Decadal Variance: Observations Versus LENS

To quantify the changes in decadal variance of the Pacific, we develop an index that captures the ENSO-like decadal variability that emerges from the PMM/ENSO interaction hypothesis. This index, which we will refer to as the progression (PROG) index, is designed to capture the progression associated with the growing, peak and decaying phases of the PDV (Di Lorenzo et al., 2015), namely, the interaction between PMM in extratropics (growth), ENSO amplification in the tropics and teleconnections to extratropics (peak phase), and the extratropical decay. The progression is typically phase locked with the seasonal cycles. For the North Pacific, a strong winter expression of the North Pacific Oscillation (NPO) (Linkin & Nigam, 2008; Rogers, 1981) will imprint an SST anomaly, which in the midlatitude [30°N–60°N] is characterized by the North Pacific Gyre Oscillation (NPGO) pattern (Chhak et al., 2009; Di et al., 2008). In the subtropics [10°N–30°N], the reduction of trade winds associated with the NPO activates the PMMs (Chang et al., 2007), which typically grow during the spring and lead to an SST anomaly in the tropics [10°S–10°N] toward the end of spring and beginning of summer. In the tropics, these anomalies favor the development of ENSO, which grows during the summer and fall and peaks in the winter. The ENSO teleconnections that follow imprint the ENSO signature into the midlatitude during the fall and the following winter [30°N–60°N].

To capture this time/space progression of the anomalies, we obtain the PROG index by computing the first Empirical Orthogonal Function (EOF) of combined raw (unfiltered) data that consist of winter (defined as December-January-February or DJF) SST anomalies (SSTa) in the midlatitude [30°N–60°N] a year prior ENSO (lag = −1 year), spring (defined as March-April-May or MAM) SSTa in the subtropics [10°N–30°N] at lag = −1 year, fall (defined as September-October-November or SON) SSTa in the tropics [10°S–10°N] at lag = −1 year, and finally winter SSTa in the midlatitude at lag zero. To recover the PMM footprint in winter and spring SSTa at lag = −1 year, we linearly remove a commonly used ENSO index (cold tongue index, SSTa averaged over 6°S–6°N and 180°W–90°W) prior to the EOF analysis. This allows for the extraction of the PMM pattern in the winter/spring preceding ENSO as discussed in Chang et al. (2007). In the observation, this modal decomposition results in a first principal component of annual values (i.e., PROG index) that explains ~67% of the variance and tracks closely both PDV temporal variations (Figure 1b) and seasonally based spatial evolution (Figure 2a). Given that the PROG index is defined using an EOF analysis that maximizes variance but does not enforce the causality in the transition patterns from ENSO precursors to ENSO successors, we conducted additional tests. Specifically, we verified that the EOF patterns of the progression are consistent with the patterns obtained by lead/lag regression maps of the Niño3.4 index with SST and wind anomaly

between −12 and +12 months (see section S1 in the supporting information). We also developed a Monte Carlo approach to show that the observed order of the SSTa sequences (e.g., causality) is required in order to capture the largest fraction of the variance throughout the DJF to DJF + 1 period.

We test the skill of the PROG index annual values in capturing PDV temporal variations by comparing the 8 year low-passed PROG index with the PDV index computed as Zhang et al. (1997), which is defined as the PC1 of 8 year low-passed monthly SST (Figure 1b). The high and significant correlation between the PROG and PDV indices (R = 0.84) allow us to use the PROG index as a diagnostic tool to (i) test the PMM/ENSO interaction decadal framework in climate models and (ii) quantify if the PDV variance is changing under anthropogenic climate change. The significance of the correlation coefficients throughout the study is estimated by computing empirical probability density functions (EPDFs) for the correlation coefficient of two red-noise time series which have the same lag-1 autoregression coefficient of those estimated in the original signals. We assess the 99% significance levels using an EPDF obtained from 10,000 realizations of random red-noise time series. A similar approach is used to assess the significance of the trend.

An examination of the observed evolution of PDV variance inferred from the 20 year running standard deviation (STD) of the PROG index shows a marked trend in both observational products (Figure 2b; it shows only the ERSST data; results for HadISST data set are not shown), raising the question of whether this trend is part of a centennial-scale (or longer) natural fluctuation or if it is linked to the anthropogenic forcing. To explore the significance of these trends and their driving mechanisms, we look at the LENS projections, which span from 1920 to 2100 and are forced by the RCP8.5 radiative forcing scenario after 2005.

Following the same approach used for the observational data set (Figure 1b), for each LENS member we compare the 8 year low-passed PROG index with the PDV index computed as in Zhang et al. (1997). The resultant mean correlation of R = 0.82 shows that the PROG index captures the ENSO-like decadal variability. We then inspect the ensemble mean pattern (i.e., average of each individual pattern) associated with the phases of the progression in the models and compare it with observations. The different phases are revealed by regressing SST and sea level pressure (SLP) anomalies onto the PROG index (Figure 2a). In the winter prior to ENSO, DJF (lag = −1 year), we find patterns characterized by large regression coefficients in the North Pacific region resembling the NPGO-like and the NPO-like pattern, respectively, for SST and SLP regressions. These patterns evolve in spring, MAM (lag = −1 year), in a stronger NPO-like pattern associated with a clear PMM signature in the SST. These ENSO precursors, NPO and PMM, promote the onset of El Niño, and thus by fall, SON (lag = −1 year), both SST and SLP regressions are dominated by a mature phase of ENSO, which is characterized by a warm SST anomaly and a strong east-west pressure gradient anomaly in the tropical Pacific. In the following winter, DJF (0), these mature ENSO conditions begin to decay after exciting extratropical teleconnections, which energize PDO-like and Aleutian Low-like patterns in the North Pacific.

This mode progression from the NPGO/NPO-like patterns during the winter prior to ENSO to a PDO/Aleutian Low-like pattern during peak ENSO shows that the PROG index captures the seasonal and spatial evolution of the Pacific variability in both observations and model simulations. The main discrepancies of LENS with respect to the observations are (i) the stronger SST signature in the warm pool region (western equatorial pacific) during DJF (lag = −1 year) and MAM (lag = −1 year) and (ii) the very weak Aleutian Low signature in the SLP of the North Pacific region during ENSO peak phase in DJF (0). Both these discrepancies are likely due to LENS deficiencies in accurately representing ENSO and its extratropical teleconnection. For instance, the LENS tendency in overestimating the SST variability in the western equatorial Pacific is a known bias present in most global coupled models that has been linked to misrepresentation of the Bijerkness feedback (Li & Xie, 2014). Nevertheless, LENS have been extensively validated in a number of recent studies (e.g., Kay et al., 2015; Fasullo & Nerem, 2016; Li, Zhu, & Dong, 2017) and represents a valuable data set to address the question of whether or not the PDV is likely to increase under greenhouse forcing. In both observational data sets, the variance of the LENS PDV inferred from the 20 year running STD of the PROG index shows a marked trend that is consistent with the LENS response to anthropogenic forcing (Figure 2b). We can now diagnose the individual mechanisms of the PDV framework that are responsible for the PDV increase in LENS.

4. Diagnosing the Role of Meridional Mode Dynamics

To diagnose the origin of the trend in the PDV variance within the LENS, we examine the individual dynamics that are important in the progression, that is, the PMM and ENSO. For each member we compute the PMM

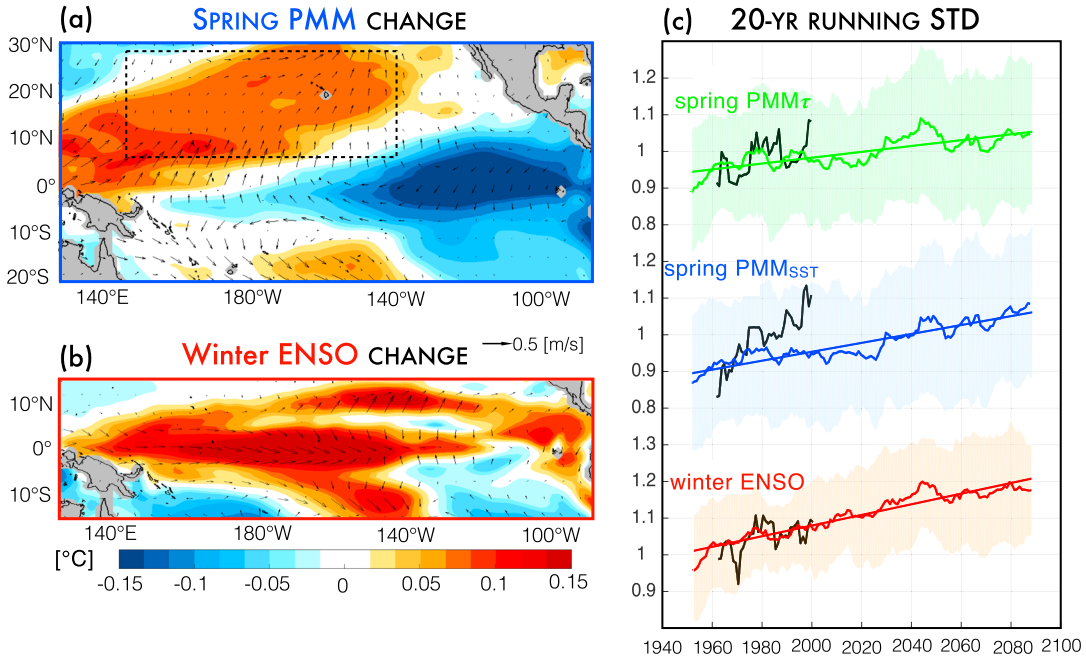

Figure 3. Projected change in the variance of PMM and ENSO. (a and b) Changes in PMM and ENSO obtained by subtracting the pattern computed during 1960–2000 (i.e., weak greenhouse forcing) to the one computed during 2060–2100 (i.e., strong greenhouse forcing). Patterns and wind vector are obtained by regressing spring PMM_{sst} and winter ENSO indices (see text for indices definitions) onto SST and wind components. Units are in °C per units of STD changes of the corresponding mode index. (c) Normalized 20 year running standard deviation of spring PMM_{sst}, spring $PMM_{?}$, and winter ENSO indices in LENS (green, blue, and red) and observations (NCEP reanalysis and ERSST v3; black).

using the definition of Chang et al. (2007) (see section 2), which results in two monthly mean indices: an SST-based index, PMM_{sst}, and a 10 m winds-based index, $PMM_{?}$. The ENSO index is instead computed as the leading PC1 of monthly mean tropical Pacific ([120°E–80°W, 20°S–20°N]) SSTs.

The cross correlation between the monthly mean PMM indices and the ENSO index confirms a known relationship in which the spring PMM index leads the winter ENSO index (R = .38 when the PMM index leads ENSO by 9 months; Figure S3 in the supporting information). To explore if this coupling between the PMM and ENSO is changing under anthropogenic forcing, we compute the correlation between the PMM_{sst} index during spring and the ENSO index during the following winter (winter defined here as DJF mean; Figure 4b). We compare the coupling between two periods, one with weak and one with strong anthropogenic forcing (i.e., 1920–1960 versus 2060–2100). We find a moderate but robust increase, 21 out of 30 members, in the ensemble mean of ~19% (R = 0.48 versus R = 0.57) during the later period. Thus, if LENS projections are correct and we assume that each member of the ensemble is as likely to occur as the real climate, the increase in the PMM-ENSO coupling has a 70% chance of occurrence. Moreover, the 20 year running variance of spring PMM_{sst} and $PMM_{?}$ reveals a significant trend in both observations and LENS (Figure 3c), with the SST response (spring PMM_{sst}) being larger than the wind stress response (spring $PMM_{?}$). This amplification in the spring PMM_{sst} variance relative to spring $PMM_{?}$ variance is consistent with the red-noise paradigm for the ocean-atmosphere interaction in which the ocean memory leads to an amplification of the atmospheric variance (Frankignoul & Hasselmann, 1977). Since the spring PMM_{sst} index captures the oceanic expression of the ocean-atmosphere coupled PMM, it is expected for this index to have more low-frequency power than the spring $PMM_{?}$, which captures the atmospheric expression of the coupled mode. In both LENS and observation, the trend in the variance of the spring PMM indices is accompanied by a marked trend in the 20 year running variance of winter ENSO (Figure 3c). These trends in the variance of spring PMM and winter ENSO are statistically significant in the ensemble mean of LENS but not in the observation, for which the record is too short to pass the significance test. In the model, the trends in the variance are accompanied by an increase in the spatial variance associated with each mode. This can be visualized by subtracting the pattern computed during 1960–2000 (i.e., weak anthropogenic forcing) from the one computed during 2060–2100

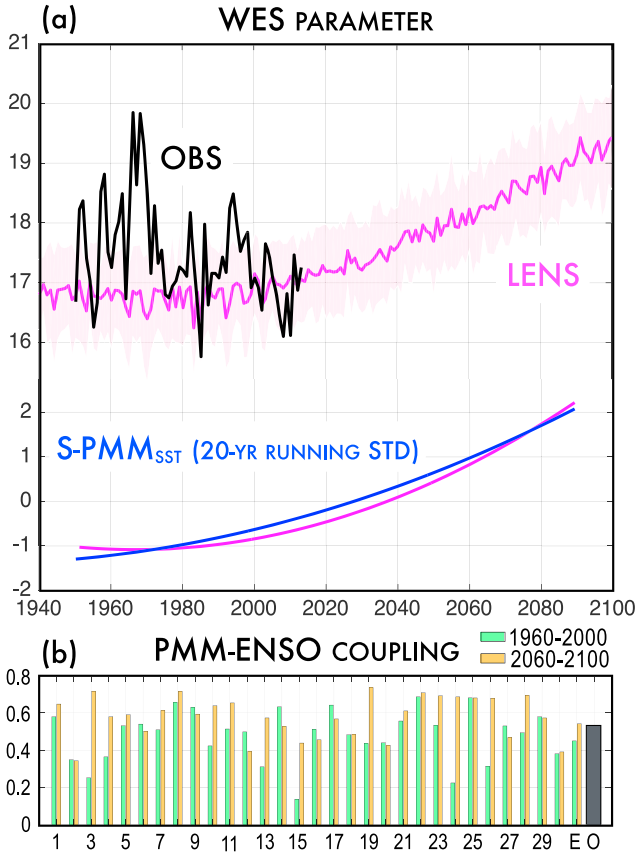

Figure 4. (a) Curves in the upper part indicate the WES parameter (Vimont, 2010) area averaged over the dashed box shown in Figure 3a in the observation (black) and LENS ensemble mean (magenta). Units are in W s m^{-3} and the shading (light magenta) indicates the 1 STD spread envelope. Curves in the lower part compare quadratic fits of the normalized ensemble mean of the WES parameter (magenta) and the 20 year running STD of the spring PMM$_{sst}$ index (blue). (b) ENSO-PMM coupling estimated as correlation between spring PMM$_{sst}$ and winter ENSO indices (see text for indices definitions). Correlation computed during 1920–1960 (green bars) and 2060–2100 (orange bars) for each LENS member (#), the ensemble mean (E), and the observations (O; 1960–2000).

(i.e., strong anthropogenic forcing) (Figures 3a and 3b). The patterns are obtained by regressing the spring PMM$_{sst}$ and winter ENSO indices onto SST and wind components.

Although ENSO variance has several contributions (e.g., westerly wind bursts, Harrison & Vecchi, 1997, and Madden-Julian Oscillation, Zhang & Gottschalck, 2002), the consistent slope between PMM and ENSO variance (Figure 3c) supports the hypothesis that the increase in the PMM variance resulting from anthropogenic forcing is an important contributor to the increase in ENSO variance. There are several mechanisms that can amplify the PMM and increase its variance: (i) increase in the feedback (i.e., WES) between ocean and atmosphere that leads to larger growth of the mode and (ii) increase in the variance of the extratropical atmospheric stochastic noise (i.e., NPO activity) that activates and energizes the PMM. In LENS, the increase in the PMM variance is consistent with an intensification of the WES feedback associated with changes in the background state. The nature of the WES feedback prevents its direct and precise quantification, but nevertheless, Vimont (2010) proposed to use the change in latent heat flux per unit change in zonal wind speed as estimation of the WES feedback activity. Specifically, upon linearization of the standard bulk formula for the latent heat flux, he derived the so-called WES parameter (WESp),

$$\mathrm{WESp} = \frac{\partial \mathrm{LH}}{\partial u} = \mathrm{LH}\frac{u}{|w|^2}$$

where LH is the latent heat flux, u the zonal wind speed, and $|w|$ the total wind speed ($|w| = \sqrt{(u^2 + v^2 + w^2)}$). We use the WESp to characterize this air-sea interaction since a large latent heat flux sensitivity to zonal wind variation is a necessary condition for an intense WES feedback in the subtropical Pacific. In both observation and LENS, we computed the spatially averaged WESp in the region where the PMM is more active (i.e., dashed box shown in Figure 3a). The time series of the WESp from LENS (Figure 4a) exhibits quadratic growth over the period 1960–2100, with a clear and significant trend emerging after 2020, and no significant trend prior 2000. Consistent with the WESp, a closer look at the trend lines in the spring PMM variance (Figure 3c) also shows that most of the increase occurs after 2020. This association is confirmed by comparing a quadratic fit of the WESp and spring PMM$_{sst}$ variance (Figure 4a).

5. Summary and Discussion

Using SST observations over the period 1920–2015, we find that the variance of the El Niño-like decadal variability in the Pacific basin has increased by ~30%, with a significant contribution from the North PMM. Combining available observations with a large ensemble of anthropogenic-forced model simulations (i.e., LENS), we offer evidence that the observed intensification in the PDV activity is consistent with anthropogenic-forced changes in the interaction between tropical and extratropical Pacific modes, namely, ENSO and PMM. These mode interactions represent the core of a dynamical framework proposed by Di Lorenzo et al. (2015) to explain the nature of the PDV as a progression of Pacific modes (Figure 1). The statistical characterization of the mode progression in both observations and model outputs reveals a substantial intensification of the dynamics that energize the PDV (Figure 2). Specifically, ENSO and the PMM show a significant trend in variance (Figure 3c) that is accompanied in LENS by an increase in the coupling between the two modes (Figure 4b). A diagnostic of the LENS suggests that these changes are significantly linked to anthropogenic forcing, which amplifies the variance of the PMM in subtropical and tropical regions. This amplification is consistent with an intensification of the winds-evaporation-SST thermodynamic feedback (i.e., WES) in the region of the North PMM. The WES, which controls the growth rate of the PMM SSTa (e.g., Vimont, 2010), exhibits an exponential increase in amplitude because of the nonlinear relationship

between SSTa and evaporation in a warming mean climate (Gill, 1980; Lindzen & Nigam, 1987). The increase in PMM amplitude also leads to a small but significant increase in coupling between PMM and ENSO in the CESM-LENS, a result that is consistent with previous studies suggesting that the link between the North Pacific ENSO precursor patterns (e.g., PMM) and ENSO increases under enhanced greenhouse warming (e.g., Wang et al., 2013, 2014). Although these results suggest an important role of the PMM dynamics, there are mechanisms other than PMM that can energize the decadal variance of Pacific SSTs. For instance, Wang et al. (2013) linked the increase in the PDV to greenhouse-forced changes in the relationship between ENSO and western North Pacific SST anomalies. Furthermore, by means of modeling experiments, Zhou et al. (2014) found that regardless of changes in the amplitude and spatial pattern of ENSO, the projected warming in the ENSO region will result in an overall increase in variance of ENSO teleconnections and hence of the oceanic response in the extratropics.

The analysis presented here provides support to the hypothesis that anthropogenic forcing may lead to an amplification of PDV through a strengthening of the PMM via the WES. However, the lack of a detectable trend in the WES parameter in the observational record does not allow for a clear attribution of the recent trends in PDV to anthropogenic forcing. According to the LENS, the trend in the WES begins to emerge in the period 2000–2020. Moreover, the computation of the WES parameter involves higher-order statistics of quantities such as latent heat and wind speed that are not well constrained in observation. While this is especially true for estimates before the satellite era, even remote sensing-based estimates present a substantial uncertainty, which in the case of the latent heat flux may be on the order of 20% or larger (Jiang et al., 2004, and reference therein). The ensemble mean statistics from the LENS are very clear in projecting an increase in WES as a response to a warmer mean state. We anticipate that an amplification of this feedback in the next one or two decades will be accompanied by an intensification in both PMM and ENSO activity. In this respect, it is plausible that the record-breaking PMM index recorded in spring 2015 (https://www.esrl.noaa.gov/psd/data/timeseries/monthly/PMM/)), followed by one of the strongest El Niño events ever recorded (winter 2016/2017) (e.g., Hu & Fedorov, 2017), represents a manifestation of this ongoing intensification.

Acknowledgments

The authors thank Shoshiro Minobe for valuable contributions in the review process. They also thank an anonymous reviewer for constructive criticisms that significantly improved the manuscript. E. D. L. and G. L. acknowledge the support of the NSF-OCE 132022 and NSF-OCE 1419292. G. L. was partially supported by the Domenica Rea D'Onofrio Fellowship. We thank the National Center for Atmospheric Research for producing and making available the results from the CESM Large Ensemble Project http://www.cesm.ucar.edu/projects/community-projects/LENS/data-sets.html. Observational SST data were obtained from https://www.esrl.noaa.gov/psd/data/gridded/data.noaa.ersst.v3.html (ERSSTv3) and https://www.metoffice.gov.uk/hadobs/hadisst/data/download.html (HadiSST).

References

Alexander, M. A., Vimont, D. J., Chang, P., & Scott, J. D. (2010). The impact of extratropical atmospheric variability on ENSO: Testing the seasonal Footprinting mechanism using coupled model experiments. *Journal of Climate*, *23*(11), 2885–2901. https://doi.org/10.1175/2010JCLI3205.1

Anderson, B. T. (2003). Tropical Pacific sea-surface temperatures and preceding sea level pressure anomalies in the subtropical North Pacific. *Journal of Geophysical Research*, *108*(D23), 4732. https://doi.org/10.1029/2003JD003805

Anderson, B. T., Perez, R. C., & Karspeck, A. (2013). Triggering of El Niño onset through trade wind-induced charging of the equatorial Pacific. *Geophysical Research Letters*, *40*, 1212–1216. https://doi.org/10.1002/grl.50200

Chang, P., Zhang, L., Saravanan, R., Vimont, D. J., Chiang, J. C. H., Ji, L., … Tippett, M. K. (2007). Pacific meridional mode and El Niño–southern oscillation. *Geophysical Research Letters*, *34*, L16608. https://doi.org/10.1029/2007GL030302

Chavez, F. P., Ryan, J., Lluch-Cota, S. E., & Niquen, M. (2003). From anchovies to sardines and back: Multidecadal change in the Pacific Ocean. *Science*, *299*(5604), 217–221. https://doi.org/10.1126/science.1075880

Chhak, K. C., Di Lorenzo, E., Schneider, N., & Cummins, P. F. (2009). Forcing of low-frequency ocean variability in the northeast Pacific. *Journal of Climate*, *22*(5), 1255–1276. https://doi.org/10.1175/2008JCLI2639.1

Chiang, J. C. H., & Vimont, D. J. (2004). Analogous Pacific and Atlantic meridional modes of tropical atmosphere-ocean variability. *Journal of Climate*, *17*(21), 4143–4158. https://doi.org/10.1175/JCLI4953.1

Delworth, T. L., & Mann, M. E. (2000). Observed and simulated multidecadal variability in the Northern Hemisphere. *Climate Dynamics*, *16*(9), 661–676. https://doi.org/10.1007/s003820000075

Di Lorenzo, E., & Mantua, N. (2016). Multi-year persistence of the 2014/15 North Pacific marine heatwave. *Nature Climate Change*, *6*(11), 1042–1047. https://doi.org/10.1038/nclimate3082

Di Lorenzo, E., Schneider, N., Cobb, K. M., Franks, P. J. S., Chhak, K., Miller, A. J., … Rivière, P. (2008). North Pacific Gyre Oscillation links ocean climate and ecosystem change. *Geophysical Research Letters*, *35*, L08607. https://doi.org/10.1029/2007GL032838

Di Lorenzo, E., Liguori, G., Schneider, N., Furtado, J. C., Anderson, B. T., & Alexander, M. A. (2015). ENSO and meridional modes: A null hypothesis for Pacific climate variability. *Geophysical Research Letters*, *42*, 9440–9448. https://doi.org/10.1002/2015GL066281

Fasullo, J. T., & Nerem, R. S. (2016). Interannual variability in global mean sea level estimated from the CESM large and last millennium ensembles. *Water-Sui*, *8*(11).

Frankignoul, C., & Hasselmann, K. (1977). Stochastic climate models. Part II: Application to sea surface temperature anomalies and thermocline variability. *Tellus*, *29*, 289–305.

Gershunov, A., & Barnett, T. P. (1998). Interdecadal modulation of ENSO teleconnections. *Bulletin of the American Meteorological Society*, *79*(12), 2715–2725.

Gill, A. E. (1980). Some simple solutions for heat-induced tropical circulation. *Quarterly Journal of the Royal Meteorological Society*, *106*(449), 447–462. https://doi.org/10.1002/qj.49710644905

Harrison, D. E., & Vecchi, G. A. (1997). Westerly wind events in the tropical Pacific, 1986–95. *Journal of Climate*, *10*(12), 3131–3156. https://doi.org/10.1175/1520-0442(1997)010%3C3131:WWEITT%3E2.0.CO;2

Hu, S. N., & Fedorov, A. V. (2017). The extreme El Niño of 2015–2016 and the end of global warming hiatus. *Geophysical Research Letters*, *44*, 3816–3824. https://doi.org/10.1002/2017GL072908

Hurrell, J., Holland, M. M., Gent, P. R., Ghan, S., Kay, J. E., Kushner, P. J., … Marshall, S. (2013). The Community Earth System Model: A framework for collaborative research. *Bulletin of the American Meteorological Society*, *94*(9), 1339–1360. https://doi.org/10.1175/BAMS-D-12-00121.1

Jiang, L., Islam, S., & Carlson, T. (2004). Uncertainties in latent heat flux measurement and estimation: Implications for using a simplified approach with remote sensing data. *Canadian Journal of Remote Sensing*, *30*(5).

Kalnay, E., Kanamitsu, M., Kistler, R., Collins, W., Deaven, D., Gandin, L., … Joseph, D. (1996). The NCEP/NCAR 40-year reanalysis project. *Bulletin of the American Meteorological Society*, *77*(3), 437–471. https://doi.org/10.1175/1520-0477(1996)077%3C0437:TNYRP%3E2.0.CO;2

Kay, J. E., Deser, C., Phillips, A., Mai, A., Hannay, C., Strand, G., … Vertenstein, M. (2015). The Community Earth System Model (CESM) large ensemble project a community resource for studying climate change in the presence of internal climate variability. *Bulletin of the American Meteorological Society*, *96*(8), 1333–1349. https://doi.org/10.1175/BAMS-D-13-00255.1

Li, G., & Xie, S. P. (2014). Tropical biases in CMIP5 multimodel ensemble: The excessive equatorial Pacific cold tongue and double ITCZ problems. *Journal of Climate*, *27*(4), 1765–1780. https://doi.org/10.1175/JCLI-D-13-00337.1

Li, J., Zhu, Z. W., & Dong, W. J. (2017). Assessing the uncertainty of CESM-LE in simulating the trends of mean and extreme temperature and precipitation over China. *International Journal of Climatology*, *37*(4), 2101–2110. https://doi.org/10.1002/joc.4837

Lindzen, R. S., & Nigam, S. (1987). On the role of sea-surface temperature-gradients in forcing low-level winds and convergence in the tropics. *Journal of the Atmospheric Sciences*, *44*(17), 2418–2436. https://doi.org/10.1175/1520-0469(1987)044%3C2418:OTROSS%3E2.0.CO;2

Linkin, M. E., & Nigam, S. (2008). The North Pacific Oscillation–West Pacific teleconnection pattern: Mature-phase structure and winter impacts. *Journal of Climate*, *21*(9), 1979–1997. https://doi.org/10.1175/2007JCLI2048.1

Mantua, N. J., Hare, S. R., Zhang, Y., Wallace, J. M., & Francis, R. C. (1997). A Pacific interdecadal climate oscillation with impacts on salmon production. *Bulletin of the American Meteorological Society*, *78*(6), 1069–1079. https://doi.org/10.1175/1520-0477(1997)078%3C1069:APICOW%3E2.0.CO;2

Meehl, G. A., & Teng, H. (2012). Case studies for initialized decadal hindcasts and predictions for the Pacific region. *Geophysical Research Letters*, *39*, L22705. https://doi.org/10.1029/2012GL053423

Rayner, N. A., Parker, D. E., Horton, E. B., Folland, C. K., Alexander, L. V., Rowell, D. P., … Kaplan, A. (2003). Global analyses of sea surface temperature, sea ice, and night marine air temperature since the late nineteenth century. *Journal of Geophysical Research*, *108*(D14), 4407. https://doi.org/10.1029/2002JD002670

Roemmich, D., & Mcgowan, J. (1995). Climatic warming and the decline of zooplankton in the California current (Vol 267, Pg 1324, 1995). *Science*, *268*(5209), 352–353. https://doi.org/10.1126/science.268.5209.352-b

Rogers, J. C. (1981). The North Pacific Oscillation. *Journal of Climatology*, *1*(1), 39–57. https://doi.org/10.1002/joc.3370010106

Smith, T. M., & Reynolds, R. W. (2005). A global merged land-air-sea surface temperature reconstruction based on historical observations (1880–1997). *Journal of Climate*, *18*(12), 2021–2036. https://doi.org/10.1175/JCLI3362.1

Vimont, D. J. (2010). Transient growth of thermodynamically coupled variations in the tropics under an equatorially symmetric mean. *Journal of Climate*, *23*(21), 5771–5789. https://doi.org/10.1175/2010JCLI3532.1

Wang, S. Y., Hipps, L., Gillies, R. R., & Yoon, J. H. (2014). Probable causes of the abnormal ridge accompanying the 2013–2014 California drought: ENSO precursor and anthropogenic warming footprint. *Geophysical Research Letters*, *41*, 3220–3226. https://doi.org/10.1002/2014GL059748

Wang, S. Y., L'Heureux, M., & Yoon, J. H. (2013). Are greenhouse gases changing ENSO precursors in the western North Pacific? *Journal of Climate*, *26*(17), 6309–6322. https://doi.org/10.1175/JCLI-D-12-00360.1

Zhang, C. D., & Gottschalck, J. (2002). SST anomalies of ENSO and the Madden-Julian oscillation in the equatorial Pacific. *Journal of Climate*, *15*(17), 2429–2445. https://doi.org/10.1175/1520-0442(2002)015%3C2429:SAOEAT%3E2.0.CO;2

Zhang, H., Clement, A., & Di Nezio, P. (2014). The South Pacific meridional mode: A mechanism for ENSO-like variability. *Journal of Climate*, *27*(2), 769–783. https://doi.org/10.1175/JCLI-D-13-00082.1

Zhang, Y., Wallace, J. M., & Battisti, D. S. (1997). ENSO-like interdecadal variability: 1900–93. *Journal of Climate*, *10*(5), 1004–1020. https://doi.org/10.1175/1520-0442(1997)010%3C1004:ELIV%3E2.0.CO;2

Zhou, Z.-Q., Xie, S.-P., Zheng, X.-T., Liu, Q., & Wang, H. (2014). Global warming-induced changes in El Niño teleconnections over the North Pacific and North America. *Journal of Climate*, *27*(24), 9050–9064. https://doi.org/10.1175/JCLI-D-14-00254.1